Available online at www.sciencedirect.com
SCIENCE DIRECT®
Journal of Solid State Chemistry 179 (2006) 532–537
JOURNAL OF SOLID STATE CHEMISTRY
www.elsevier.com/locate/jssc

Microstructure and luminescence of transparent glass ceramic containing Er^{3+}:BaF_2 nano-crystals

Daqin Chen, Yuansheng Wang*, Yunlong Yu, En Ma, Lihua Zhou

State Key Laboratory of Structural Chemistry, Fujian Institute of Research on the Structure of Matter, Chinese Academy of Sciences, Graduate School of Chinese Academy of Sciences, Fuzhou, Fujian 350002, China

Received 19 August 2005; received in revised form 9 November 2005; accepted 9 November 2005
Available online 15 December 2005

Abstract

Transparent BaF_2–SiO_2 glass ceramics doped with different content of Er^{3+} were prepared by sol–gel method. The microstructural evolution of the samples was studied with X-ray diffraction (XRD), transmission electron microscope (TEM), absorption and infrared spectra (IR). BaF_2 nano-crystals with 2–15 nm in size, depending on the crystallization temperature, distributed homogeneously among the amorphous silica matrix. The BaF_2 lattice parameters decreased with the increasing of Er^{3+} doping, indicating the incorporation of Er^{3+} into nano-crystals, which was further confirmed by energy dispersive X-ray spectroscopy (EDS) and absorption spectra analysis. The upconversion emissions of Er^{3+} emerged under the excitation at 980 nm for glass ceramic heat-treated at 800 °C.

Keywords: Oxyfluoride glass ceramics; Sol–gel; BaF_2 nano-crystals; Upconversion

1. Introduction

Recently, oxyfluoride glass ceramics have widely been investigated as host materials for active optical ions because they have not only comparatively low phonon energies due to fluorides, but also high chemical and mechanical stabilities related to oxides [1–5]. The conventional method for fabricating glass ceramics is melt quenching, which is convenient but suffers from the compositional uncertainty of the glass due to partial evaporation of some components during high temperature melting. Sol–gel method provides a new approach to fabricate glass ceramics. It has several advantages over melt quenching: lower processing temperature, easier composition control, and better chemical homogeneity of the product [6]. Using this method, some rare earth (RE) doped transparent oxyfluoride glass ceramics with excellent optical properties have been prepared recently [7–10].

Trivalent RE doped MF_2 (M = Ba, Sr, Ca, Cd) crystals, characterized by low phonon energy and large transfer coefficient between RE ions, have been of great interest owing to their possible applications as optical materials [11,12]. However, transparent oxyfluoride glass ceramics containing MF_2 nano-crystals prepared by sol–gel method have seldom been reported to date. In this paper, we report for the first time the sol–gel preparation of Er^{3+} doped BaF_2–SiO_2 glass ceramics and the investigation results on microstructural evolution and its influence on luminescence of these materials.

2. Experimental

2.1. Sample preparation

Reagent grade of tetraethylorthosilicate (TEOS), trifluoroacetic acid (TFA), ethyl alcohol, erbium acetate, barium acetate, acetic acid, and deionized water were used as starting materials to prepare bulk xerogels with the following composition (in mol%): $x$$ErF_3$–5$BaF_2$–95$SiO_2$ (x = 0, 0.5, 1.0). Fluorination was carried out by a way similar to that reported by Fujihara et al. [13]. In summary, TEOS, diluted with equal volume of ethyl alcohol, was hydrolyzed with water and stirred for 2 h (denoted as the TEOS solution). Acetic acid was used as the catalyst. The

*Corresponding author. Fax: +86 591 8370 5402.
E-mail address: yswang@fjirsm.ac.cn (Y. Wang).

0022-4596/$ - see front matter © 2005 Elsevier Inc. All rights reserved.
doi:10.1016/j.jssc.2005.11.010

volume ratio of TEOS: H_2O: CH_3COOH was 7:2:1. The Ba^{2+} and Er^{3+} ions were introduced in the form of their acetate salts. Required amount of the salts were dissolved in TFA with molar ratio of 1:10 and a small amount of water was used to speed up the dissolving process (the resultant solution was denoted as the TFA solution). Finally, the TFA solution was dropwise added into the TEOS solution, followed by stir for 30 min at room temperature. The mixed solution was then poured into the culture vessels covered with aluminum foil to form gels, which were then aged for 2 weeks at room temperature, and finally dried at elevated temperature from 20 to 120 °C within 7 days to form the xerogels.

2.2. Structural characterization

Thermo gravimetric-differential thermal analysis (TG-DTA, STA449C) of the bulk xerogel samples was performed in air at a heating rate of 10 K/min in order to follow the thermal behavior. By heat treatment at 200, 300, 500, 700, 800, 900 and 1000 °C, respectively, for 2 h, crystallization proceeded in the xerogels, resulting in the formation of glass ceramics. To identify crystallization phase, XRD analysis was performed on an X-ray powder diffractometer (XRD, DMAX2500) with Cu$K\alpha$1 radiation. The microstructure of the samples was studied by transmission electron microscope (TEM, JEM-2010) equipped with energy dispersive X-ray spectroscope (EDS) and operated at 200 kV. TEM specimens were prepared by dispersing fine power grinded from bulk sample in ethanol, followed by ultrasonic agitation, and then deposition onto the carbon-enhanced copper grid. Infrared spectra (IR, Spectrum One) of 0.5 mol% Er^{3+} doped samples were recorded in the wave range of 2000–400 cm^{-1} by KBr method.

2.3. Optical spectroscopic measurement

Optical absorption spectra of the 0.5 mol% Er^{3+} doped samples were measured by a UV-near-infrared spectrophotometer (Lamda900) at room temperature. The luminescence was recorded on a spectrofluorimeter (FLS920) under the excitation of a 378 nm light from the 450 W stable Xenon lamp. The upconversion fluorescence signals under the excitation of a diode laser at 980 nm were detected with a PMT detector (R928). All the measurements were carried out at room temperature.

3. Results and discussion

3.1. Thermal behavior

TG-DTA curve of the xerogel doped with 0.5 mol% Er^{3+} is shown in Fig. 1. The TG curve presents a dramatic weight loss at about 300 °C attributing to the decomposition of $Ba(CF_3COO)_2$, which is regarded as a common process for oxyfluoride xerogel systems containing TFA to introduce fluorine [13–15]. At the same temperature range, a unique exothermic peak corresponding to the crystallization of BaF_2 nano-crystals confirmed by XRD analysis and TEM observation, emerges in the DTA curve.

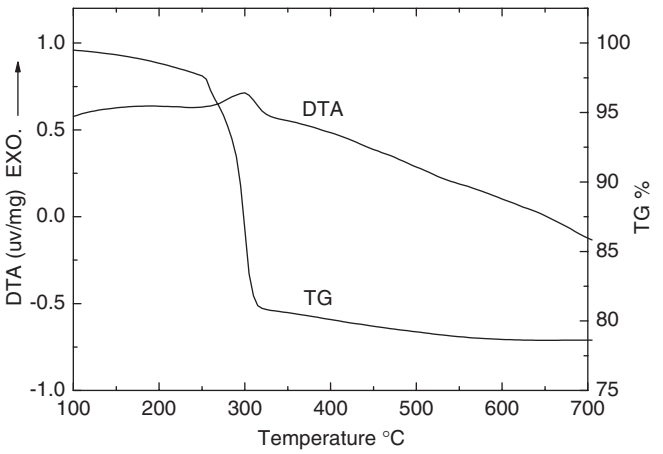

Fig. 1. TG-DTA curves of the 0.5 mol% Er^{3+} doped xerogel.

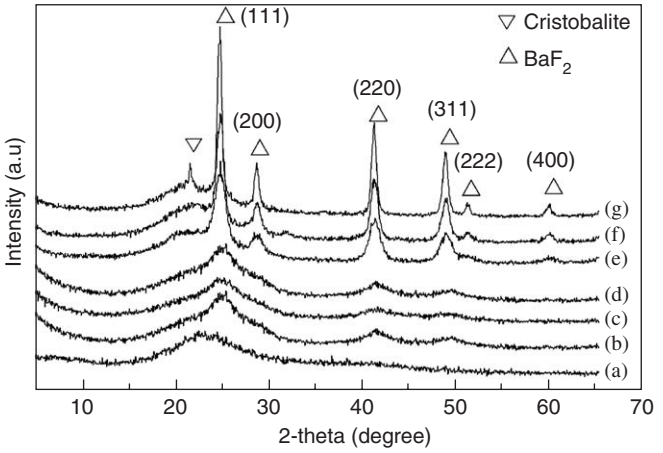

Fig. 2. XRD patterns of the 0.5 mol% Er^{3+} doped sample heat-treated at different temperature for 2 h: (a) 200 °C, (b) 300 °C, (c) 500 °C, (d) 700 °C, (e) 800 °C, (f) 900 °C and (g) 1000 °C.

3.2. XRD analysis

Fig. 2 shows the XRD patterns of the 0.5 mol% Er^{3+} doped sample heat-treated at different temperature for 2 h. The as-made xerogel and the sample heat-treated at 200 °C are amorphous. Broad peaks due to BaF_2 nano-crystals (2–4 nm in size) appear for sample heat-treated at 300 °C, which remain almost the same when the heat treatment temperature reached 700 °C, indicating good thermal stability of BaF_2 nano-crystals in this temperature range. When the temperature reaches and exceeds 800 °C, BaF_2 nano-crystals obviously grow up to about 10 nm. With the temperature further increasing to 1000 °C, besides BaF_2

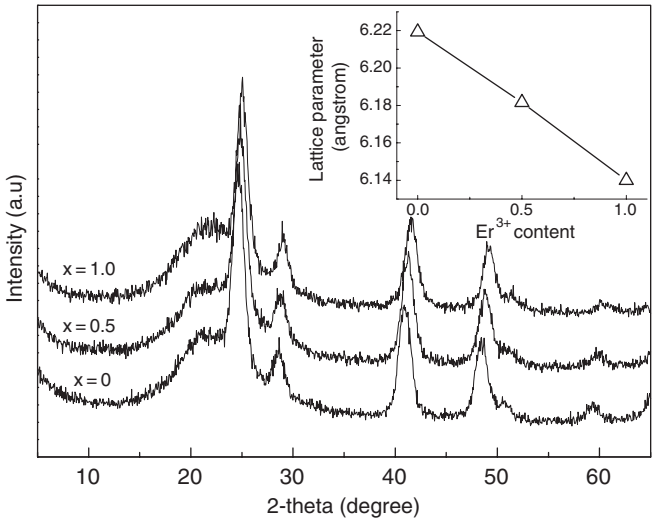

Fig. 3. XRD patterns of 800 °C heat-treated glass ceramics doped with different content of Er^{3+}. The inset shows the evolution of BaF_2 lattice parameters as a function of Er^{3+} content. The line is only as the guide for the eye.

phase, small amount of cristobalite was also precipitated from the matrix.

The XRD patterns of 800 °C heat-treated glass ceramics doped with different content of Er^{3+} are shown in Fig. 3. It is obvious that with the increasing of Er^{3+} doping, the positions of the BaF_2 diffraction peaks shift gradually towards the higher angle side, revealing the lattice contraction of BaF_2 nano-crystals, as shown in the inset of Fig. 3. It is proposed that the lattice contraction is due to the substitution of Ba^{2+} (ionic radius 1.42 Å) by Er^{3+} (ionic radius 1.00 Å) in BaF_2 lattice. Such incorporation of Er^{3+} ions into fluoride nano-crystals during its crystallization had also been detected in other oxyfluoride glass ceramics [16,17].

3.3. TEM observation

The TEM bright field image and corresponding SAED pattern in Fig. 4(a) confirm the amorphous structure of the as-made xerogel. After heat-treated at 300 °C, BaF_2 nano-crystals sized about 2–3 nm homogenously precipitated from the glass matrix. The crystalline size kept almost unchanged when the heating temperature increased to 700 °C, in consistent with the XRD results stated above. The typical microstructure of glass ceramic heat-treated at 500 °C is shown in Fig. 4(b). For glass ceramic heat-treated at 800 °C, BaF_2 nano-crystals rapidly grew up to about 10 nm, as shown in Fig. 4(c). The detailed lattice structure of a BaF_2 nano-crystal is presented by the HRTEM image in Fig. 4(d). It is worthy to mention that for all these monolith glass ceramics samples the transparency is excellent, which is important for their possible application as optical materials. The phenomenon of growth of BaF_2 nano-crystals retarded at the temperature range of 300–700 °C is noteworthy. The reason is probably due to the interfacial interaction between nano-crystals and glass matrix. Further investigation is proceeding.

EDS is commonly used to determine the composition of the micro-area. In order to reveal the distribution of Er in the sample, EDS spectra taken from the glass matrix and from an larger area containing glass matrix and several crystallites, for the 0.5 mol% Er^{3+} doped sample heat-treated at 800 °C, were obtained and shown in Fig. 5. The spectrum from the glass matrix shows high content of Si and O, and Er concentration is under detecting limit. In contrast, besides Si and O, the spectrum from the area containing glass matrix and several crystallites presents some contents of Ba, F and Er. Combined with the results of XRD, it is concluded that Er^{3+} ions are mainly concentrated in the BaF_2 nano-crystals.

3.4. Spectral analysis

The IR spectra of the 0.5 mol% Er^{3+} doped samples as a function of heat treatment temperature in the wavenumber range of 400–2000 cm^{-1} are shown in Fig. 6. The bands at about 1090, 800 and 476 cm^{-1} correspond to the Si–O–Si stretching or bending modes [18]. The intensity of Si–OH stretching peak around 960 cm^{-1} [19] marked by square decreases with increasing of the temperature, and finally disappears at 800 °C. The band at around 1650 cm^{-1} marked by arrow is assigned to the bending mode of water molecules [20], and their intensity also decreases with increasing of the temperature. Some additional small bands marked by circle in the range of 600–1500 cm^{-1} for the xerogel sample are due to the absorption by the organic groups such as $–COO^-$, C–F and C–H, etc. [21], which disappear at 500 °C.

The absorption spectra in the range from 300 to 800 nm for as-made xerogel and glass ceramic samples with identical thickness are shown in Fig. 7. The absorption peaks, corresponding to the transitions from Er^{3+} ground state $^4I_{15/2}$ to the various excited states, are marked in the figure. Compared with those in the xerogel sample, the optical densities for hypersensitive transitions of $^4I_{15/2} \rightarrow {}^4G_{11/2}$ and $^4I_{15/2} \rightarrow {}^2H_{11/2}$ [22] in the glass ceramics obviously decreased. The as-made xerogel showed amorphous structure as verified by XRD and TEM. Therefore, the ligand field environment of Er^{3+} ions was altered after crystallization, i.e., from dominating amorphous silica environment to crystalline fluoride one, since Er^{3+} ions incorporated into the precipitated BaF_2 nano-crystals. The intensity hypersensitivity of transitions from ground state to $^4G_{11/2}$ and $^2H_{11/2}$ can be characterized by the Judd–Ofelt intensity parameter Ω_2. The value of Ω_2 decreases when Er^{3+} environment changes from amorphous silica to crystalline fluoride, as reported in our previous paper for the similar glass ceramic system containing CaF_2 nano-crystals [23], which explains the decrease of the absorption optical densities for the two hypersensitive transitions after crystallization.

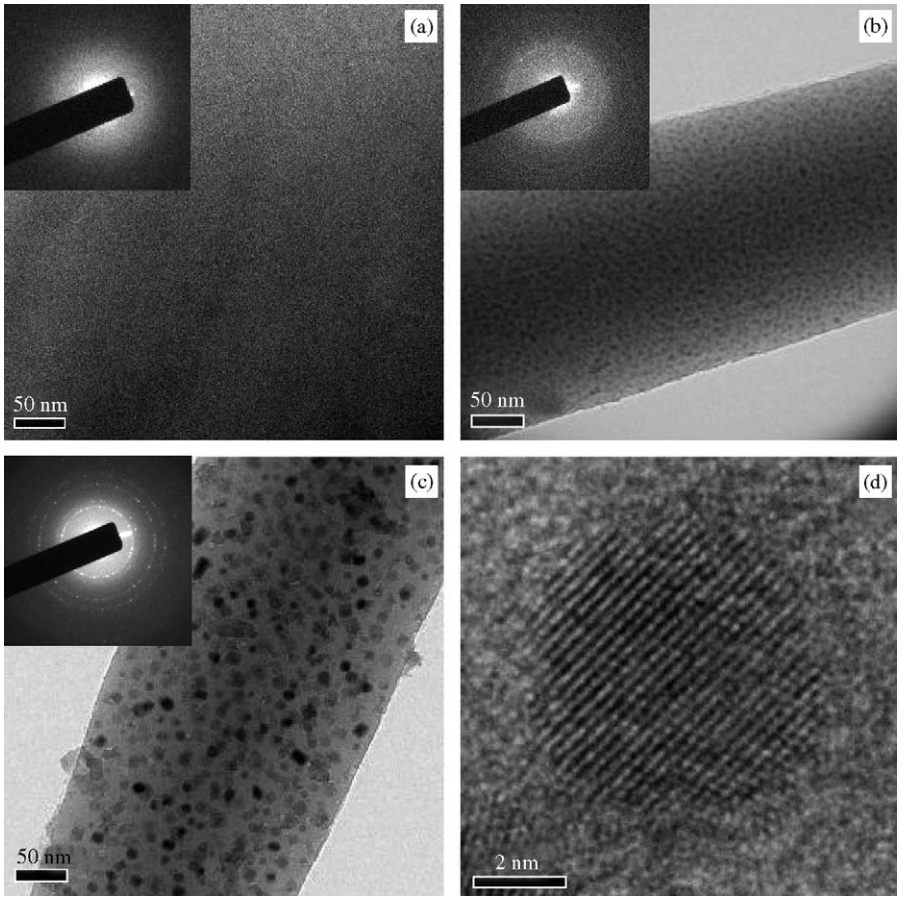

Fig. 4. TEM micrographs and corresponding selected area electron diffraction (SAED) patterns of the 0.5 mol% Er^{3+} doped BaF_2–SiO_2 system: (a) xerogel, (b) 500 °C and (c) 800 °C heat treated; (d) HRTEM image of an individual BaF_2 nano-crystal shown in (c).

3.5. Luminescence

The luminescence spectra under 378 nm excitation of the 0.5 Er^{3+} mol% doped as-made xerogel and glass ceramics heat-treated at 500 and 800 °C, respectively, are shown in Fig. 8. The luminescence spectra for the as-made xerogel and glass ceramic heat-treated at 500 °C do not present any emission bands. However, two characteristic emission bands corresponding to $^2H_{11/2}$, $^4S_{3/2} \rightarrow {}^4I_{15/2}$ and $^4F_{9/2} \rightarrow {}^4I_{15/2}$ transitions were recorded for glass ceramic sample heat-treated at 800 °C. These results were due to the elimination of Si–OH bond and other organic groups and the decrease of residual water molecules verified by the IR spectra.

By exciting at 980 nm with a diode laser, the upconversion emissions of Er^{3+} were recorded for glass ceramic heat-treated at 800 °C, as shown in Fig. 9. The two emission bands are assigned, respectively, to the transitions of $^2H_{11/2}$, $^4S_{3/2} \rightarrow {}^4I_{15/2}$ (green luminescence) and $^4F_{9/2} \rightarrow {}^4I_{15/2}$ (red luminescence). It is well known that the probability for non-radiative decay decreases exponentially with the number of required phonons [24]. The energy gap between $^4I_{11/2}$ and $^4I_{13/2}$ is about 3700 cm^{-1}, and approximate ten phonons are required to produce non-radiative decay from $^4I_{11/2}$ to $^4I_{13/2}$ in fluoride nano-crystal with vibration energy about 300–400 cm^{-1} [25]. Since the Er^{3+} ions are mainly incorporated into BaF_2 nano-crystals for glass ceramics heat treated at 800 °C, the probability for non-radiative decay is thus very low, resulting in the appearance of efficient upconversion emissions.

4. Conclusion

Er^{3+} doped glass ceramics with BaF_2 nano-crystals homogenously dispersed among silica glass were prepared by sol–gel method. The EDS and XRD analyses revealed the incorporation of Er ions into BaF_2 nano-crystals during crystallization. The decrease of optical densities for the hypersensitive transitions of $^4I_{15/2} \rightarrow {}^4G_{11/2}$ and $^4I_{15/2} \rightarrow {}^2H_{11/2}$ in glass ceramics than those in precursor glass also suggested the alteration of Er^{3+} environment from amorphous silica to crystalline fluoride after crystallization. For glass ceramic heated at 800 °C, the luminescence appeared due to the elimination of Si–OH bond and the other organic groups, and the decrease of residual water molecules in the sample. Meanwhile, the efficient upconversion emissions around 545, 565 and

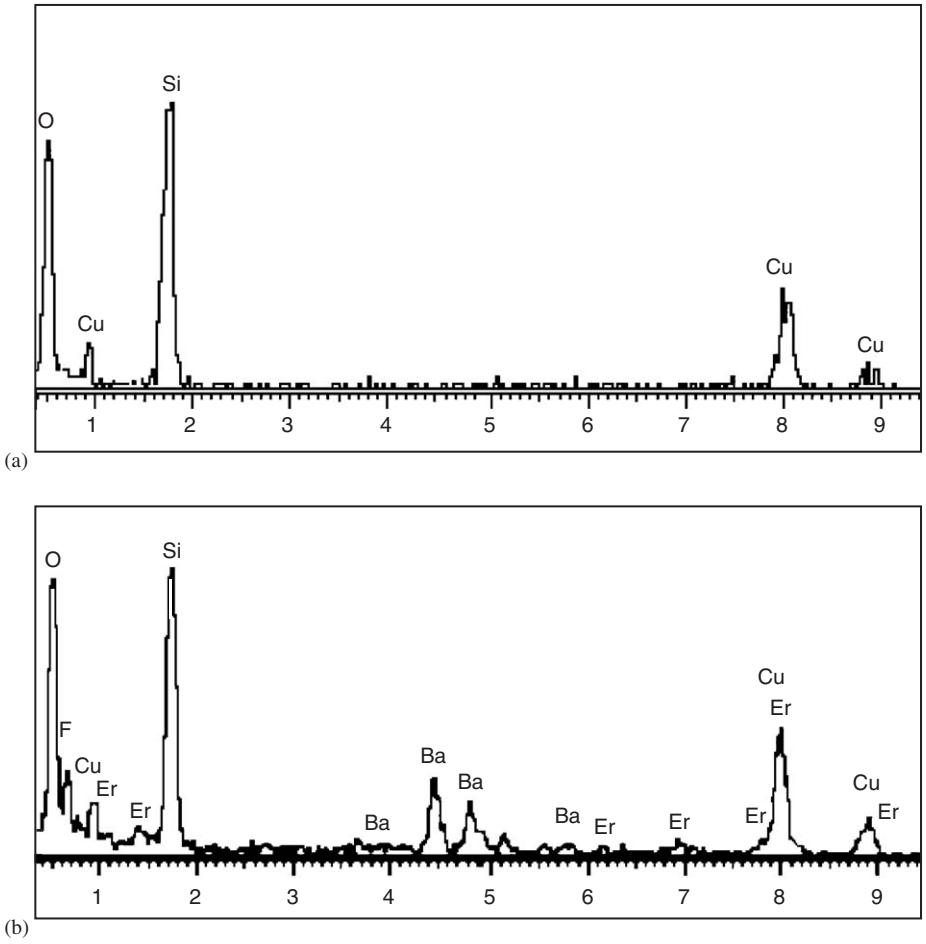

Fig. 5. EDS spectra of the 0.5 mol% Er^{3+} doped sample heat-treated at 800 °C taken from: (a) the glass matrix, and (b) an area containing glass matrix and several crystallites. (The presence of Cu element is due to the application of copper grid for TEM specimen.)

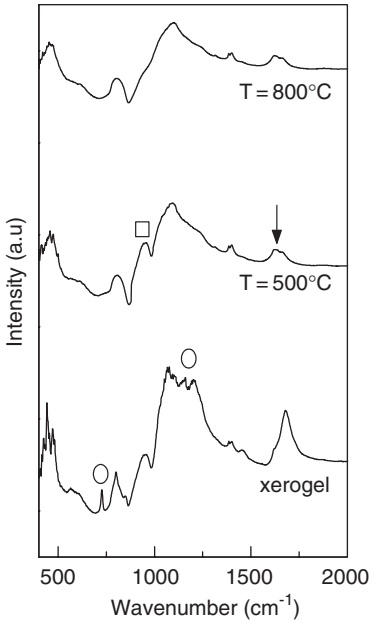

Fig. 6. IR spectra of the 0.5 mol% Er^{3+} doped samples heat-treated at different temperature.

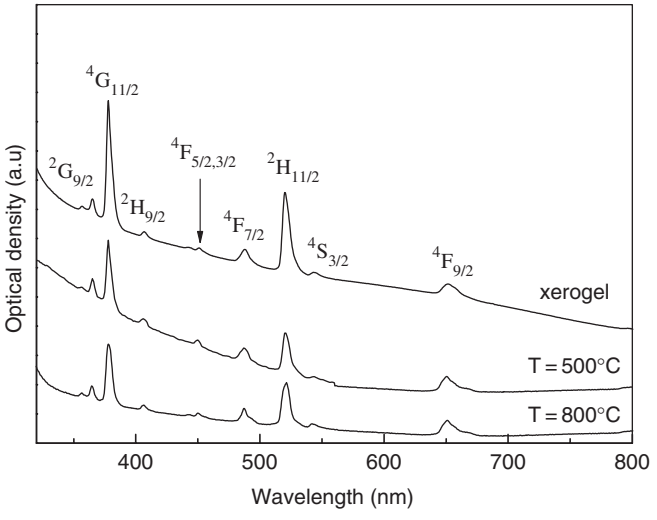

Fig. 7. Room temperature absorption spectra of the 0.5 mol% Er^{3+} doped xerogel and glass ceramics heat-treated at 500 and 800 °C, respectively.

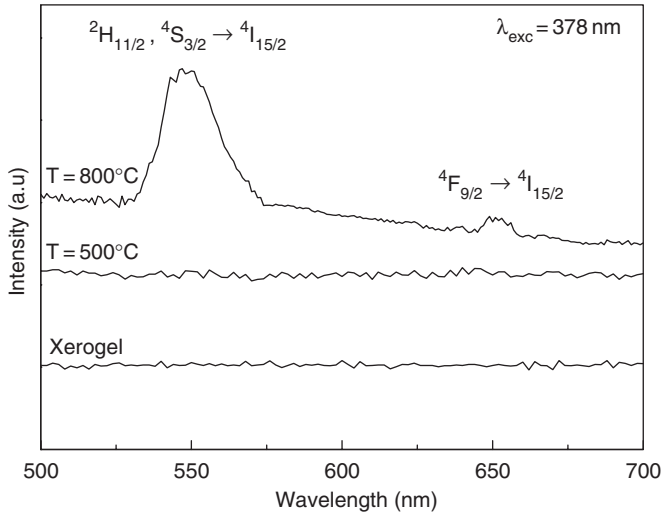

Fig. 8. The visible luminescence spectra under 378 nm excitation of the 0.5 mol% Er^{3+} doped samples heat-treated at different temperature.

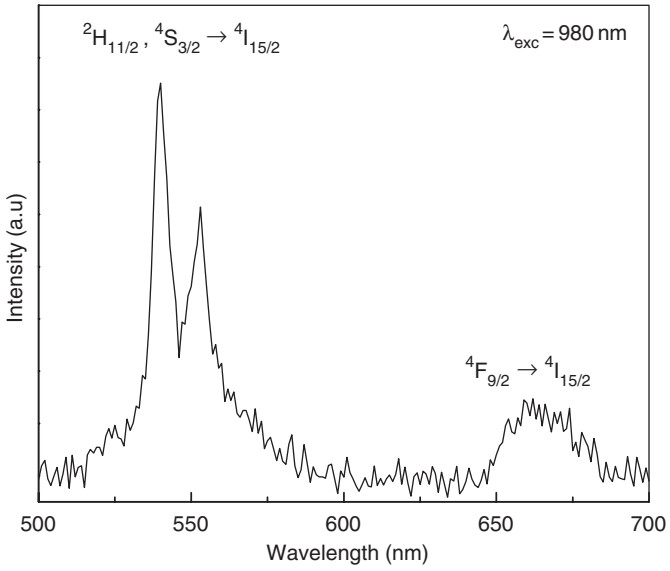

Fig. 9. Upconversion emission spectrum under 980 nm excitation in the 0.5 mol% Er^{3+} doped glass ceramic heat-treated at 800 °C.

655 nm were also recorded under 980 nm excitation due to the lower phonon energy environment of Er^{3+} ions in glass ceramic.

Acknowledgments

This work was supported by grants from the Natural Science Foundation of Fujian Province (Project No. A0320001), the Major Program on Nano-Science and Technology of Fujian Province (2005) and State Key Laboratory of Structural Chemistry of China (Project No. 050005).

References

[1] Y. Wang, J. Ohwaki, Appl. Phys. Lett. 63 (1993) 3268.
[2] M.J. Dejneka, J. Non-Cryst. Solids 239 (1998) 149.
[3] M. Mortier, G. Patriarche, J. Mater. Sci. 35 (2000) 4849.
[4] F. Lahoz, I.R. Martin, J. Mendez-Ramos, J. Chem. Phys. 120 (2004) 6180.
[5] M. Abril, M. Méndez-Ramos, I.R. Martín, U.R. Rodríguez-Mendoza, V. Lavín, A. Delgado-Torres, V.D. Rodríguez, P. Núñez, A.D. Lozano-Gorrín, J. Appl. Phys. 95 (2004) 5271.
[6] I. Jaymes, A. Douy, J. Sol–Gel Sci. Technol. 4 (1995) 7.
[7] A. Biswas, G.S. Maciel, C.S. Friend, P.N. Prasad, J. Non-Cryst. Solids 316 (2003) 393.
[8] S.J.L. Ribeiro, C.C. Araújo, L.A. Bueno, R.R. Gonçalves, Y. Messaddeq, J. Non-Cryst. Solids 348 (2004) 180.
[9] L.H. Zhou, W.Q. Luo, Y.S. Wang, F. Bao, X.H. Wang, Chin. J. Struct. Chem. 23 (2004) 1404.
[10] W.Q. Luo, Y.S. Wang, F. Bao, L.H. Zhou, X.H. Wang, J. Non-Cryst. Solids 347 (2004) 31.
[11] M. Boufard, J.P. Jouart, M.F. Joubert, Opt. Mater. 14 (2000) 73.
[12] V. Grover, S.N. Achary, S.J. Patwe, A.K. Tyagi, Mater. Res. Bull. 38 (2003) 1413.
[13] S. Fujihara, C. Mochizuki, T. Kimura, J. Non-Cryst. Solids 244 (1999) 267.
[14] M. Tada, S. Fujihara, T. Kimura, J. Mater. Res. 5 (1990) 1610.
[15] C. Rüssel, J. Non-Cryst. Solids 152 (1993) 161.
[16] M.A.P. Silva, V. Briois, M. Poulain, Y. Messaddeq, S.J.L. Ribeiro, J. Phys. Chem. Solids 64 (2003) 95.
[17] Z.J. Hu, Y.S. Wang, F. Bao, W.Q. Luo, J. Non-Cryst. Solids 351 (2005) 722.
[18] S. Chakrabarti, J. Sahu, M. Chakraborty, H.N. Acharya, J. Non-Cryst. Solids 180 (1994) 96.
[19] R.M. Parrill, C.G. Pantano, J. Appl. Phys. 68 (1990) 4225.
[20] X.H. Huang, Z.H. Chen, Mater. Res. Bull. 40 (2005) 105.
[21] S. Fujihara, S. Ono, Y. Kishiki, M. Tada, T. Kimura, J. Fluorien. Chem. 105 (2000) 65.
[22] C.K. Jorgensen, B.R. Judd, Mol. Phys. 8 (1964) 281.
[23] D.Q. Chen, Y.S. Wang, Y.L. Yu, E. Ma, Z.J. Hu, J. Phys. Condens. Matter 17 (2005) 6545.
[24] T. Miyakawa, D.L. Dexter, Phys. Rev. B 1 (1970) 1961.
[25] S. Tanabe, H. Hayashi, T. Hanada, N. Onodera, Opt. Mater. 19 (2002) 343.